

# A PARALLEL METHOD FOR SOLVING POISSON EQUATIONS WITH DIRICHLET DATA USING LOCAL BOUNDARY INTEGRAL EQUATIONS AND RANDOM WALKS \*

CHANHAO YAN<sup>†</sup>, WEI CAI<sup>‡</sup>, AND XUAN ZENG<sup>§</sup>

**Abstract.** In this paper, we will present a new approach for solving Poisson equations in general 3-D domains. The approach is based on a local computation method for the DtN mapping of the Poisson equation by combining a deterministic (local) boundary integral equation method and the probabilistic Feynman-Kac formula of PDE solutions. This hybridization produces a parallel algorithm where the bulk of the computation has no need for data communications. Given the Dirichlet data of the solution on a domain boundary, a local boundary integral equation (BIE) will be established over the boundary of a local region formed by an hemisphere superimposed on the domain boundary. By using a homogeneous Dirichlet Green's function for the whole sphere, the resulting BIE will involve only Dirichlet data (solution value) over the hemisphere surface, but both Dirichlet and Neumann data over the patch of the domain boundary intersected by the hemisphere. Then, firstly, the solution value on the hemisphere surface is computed by the Feynman-Kac formula, which will be implemented by a Monte Carlo walk on spheres (WOS) algorithm. Secondly, a boundary collocation method is applied to solve the integral equation on the aforementioned local patch of the domain boundary to yield the required Neumann data there. As a result, a local method of finding the DtN mapping is obtained, which can be used to find all the Neumann data on the whole domain boundary in a parallel manner. Finally, the potential solution in whole space can be computed by an integral representation using both the Dirichlet and Neumann data over the domain boundary.

**Key words.** DtN mapping, last-passage method, Monte Carlo method, WOS, Poisson equations

**AMS subject classifications.** 65C05, 65N99, 78M25, 92C45

**1. DtN mapping and solutions of potential equations.** The DtN mapping between the Dirichlet data (solution value) and the Neumann data (the normal derivative of the solution) of a Poisson equation is relevant in both engineering applications and mathematical study of elliptic PDEs. In the electrostatic potential problems, the surface charge distribution  $\sigma_s$  on the surface  $\partial\Omega$  of a conductor  $\Omega$ , as required in the capacitance calculation of conductive interconnects in VLSI chips, is exactly the normal derivative of the electrostatic potential  $u$  as implied from the Gauss's law for the electric field  $\mathbf{E} = -\nabla u$ , i.e.,

---

\*Submitted to SIAM J. Scientific Computing in revision on October 4, 2012. First and third authors are supported by CNSF and the second author by US NSF and DOE.

<sup>†</sup>State Key Lab. of ASIC & System Fudan Univ. Shanghai, China ([yanch@fudan.edu.cn](mailto:yanch@fudan.edu.cn))

<sup>‡</sup>Dept. of Mathematics & Statistics University of North Carolina at Charlotte, USA. ([wcai@uncc.edu](mailto:wcai@uncc.edu))

<sup>§</sup>State Key Lab. of ASIC & System Fudan Univ. Shanghai, China ([xzeng@fudan.edu.cn](mailto:xzeng@fudan.edu.cn))

$$\sigma_s = \mathbf{E} \cdot \mathbf{n}|_{\partial\Omega} = -\frac{\partial u}{\partial \mathbf{n}}|_{\partial\Omega}. \quad (1.1)$$

On the other hand, the DtN mapping also plays an important role in the study of the Poisson equations. As the inhomogeneity right-hand side of a Poisson equation is usually known, we could use a simple subtraction technique to reduce the Poisson equation to a Laplace equation, but with a modified boundary data. Therefore, in the rest of this paper we will present our method for the Laplace equation in a domain  $\Omega$  where a general Dirichlet data is given on the boundary  $\partial\Omega$ . If we are able to compute the Neumann data for the given Dirichlet data, namely the following DtN mapping:

$$\text{DtN: } u|_{\partial\Omega} \rightarrow \frac{\partial u}{\partial \mathbf{n}}|_{\partial\Omega}, \quad (1.2)$$

then, the solution  $u(\mathbf{x})$  at any point  $\mathbf{x}$  in the whole space can be found simply by the following integral representation,

$$u(\mathbf{x}) = \int_{\partial\Omega} G(\mathbf{x}, \mathbf{y}) \frac{\partial u(\mathbf{y})}{\partial \mathbf{n}_{\mathbf{y}}} ds_{\mathbf{y}} - \int_{\partial\Omega} \frac{\partial G(\mathbf{x}, \mathbf{y})}{\partial \mathbf{n}_{\mathbf{y}}} u(\mathbf{y}) ds_{\mathbf{y}}, \quad \mathbf{x} \in \mathbb{R}^3 \setminus \partial\Omega, \quad (1.3)$$

where  $G(\mathbf{x}, \mathbf{y})$  is the fundamental solution to the Laplace operator, namely,

$$G(\mathbf{x}, \mathbf{y}) = \frac{1}{4\pi} \frac{1}{|\mathbf{x} - \mathbf{y}|}. \quad (1.4)$$

A similar NtD mapping from Neumann data to Dirichlet data can also be defined if the Neumann data yields a unique solution to the PDE. In either case, with both Dirichlet and Neumann data at hand, the solution of a Laplace equation can be obtained by the representation formula in (1.3).

In addition to the electrostatic potential problem in the capacitance calculation, the solution of the Poisson equation or Helmholtz equations is also the main component of projection-type methods for incompressible flows [5][27], which usually involve the solution of a Helmholtz equation for the velocity field and a Poisson equation for the pressure field. Therefore, by finding the DtN or NtD mapping of the relevant elliptic PDE solutions in an efficient manner, we could produce fast numerical methods for many electrical engineering and fluid mechanics applications.

For the capacitance problems of conductors, boundary element method (BEM) or finite element method (FEM) have been used as electrostatic field solvers to compute the charge density, for example, the indirect BEM Fast-Cap [24][25], the direct BEM QMM-BEM [29], hierarchical extractors Hi-Cap and PhiCap [26][28], and the parallel adaptive finite element method the ParAFEMCap [7], etc. BEMs [2] need to discretize entire conductor surfaces, sometimes even the dielectric interfaces, into small panels, and construct a linear system by method of moments or collocation methods to be solved. These

deterministic methods are highly accurate and versatile, but are global, i.e., even if the charge density at only one point is required, a full linear system has to be constructed and solved. In general, the resulting linear algebraic systems are solved by iterative methods such as the multi-grid methods [3] or the domain decomposition methods [30], either as a solver or pre-conditioner. For integral equation discretization, the fast multipole method (FMM) [13] can be used in conjunction with a Krylov subspace iterative solver. All these solvers are  $O(N)$  in principle and iterative in nature, and require expensive surface or volume meshes. The parallel scalability of these solvers on large number of processors poses many challenges and is the subject of intensive research. In comparison, the method proposed in this paper is intrinsically parallel and has the potential of high parallel scalability.

Due to the limited memory in computers and computational time, sometimes it is impractical to obtain solutions by global methods for many engineering problems such as modern VLSI chips with millions of circuit elements. In contrast, random methods can give local solutions, which have been applied in the area of chip design industrials. For instance, the Rapid 3D and QuickCap, as the chip industry's gold standards produced by the leading EDA companies Synopsys and Magma respectively, are both random methods. The key advantage of the random methods is their localization. For example, QuickCap [8][9] can calculate the potential or charge density at only a point locally without finding the solution elsewhere. Usually, random methods are based on the Feynman-Kac formula and the potential (or charge density) is expressed as a weighted average of the boundary values [17].

The Feynman-Kac formula [11][12] relates Ito diffusion paths to the solution  $u(\mathbf{x})$  of the following general elliptic problem

$$\begin{aligned} L(u) &\equiv \sum_{i=1}^n b_i(\mathbf{x}) \frac{\partial u}{\partial x_i} + \sum_{i,j=1}^n a_{ij}(\mathbf{x}) \frac{\partial^2 u}{\partial x_i \partial x_j} = f(\mathbf{x}), \quad \mathbf{x} \in \Omega, \\ u|_{\partial\Omega} &= \phi(\mathbf{x}), \quad \mathbf{x} \in \partial\Omega. \end{aligned} \quad (1.5)$$

If  $X_t(\omega)$  is an Ito diffusion defined by the following stochastic differential equation

$$dX_t = b(X_t)dt + \alpha(X_t)dB_t, \quad (1.6)$$

where  $B_t(\omega)$  is the Brownian motion,  $[a_{ij}] = \frac{1}{2}\alpha(x)\alpha^T(x)$ , then, the following Feynman-Kac formula gives a probabilistic solution for (1.5) as

$$u(\mathbf{x}) = E^x(\phi(X_{\tau_\Omega}) + E^x[\int_0^{\tau_\Omega} f(X_t)dt]), \quad (1.7)$$

where the expectation is taken over all sample paths  $X_{t=0}(\omega) = \mathbf{x}$  and  $\tau_\Omega$  is the first hit time (or exit time) of the domain  $\Omega$ . This representation holds for general linear elliptic PDEs. However, for the purpose of this paper, we will only consider the Laplace equations.

For the Laplace equation ( $f = 0$ ), the Ito diffusion is just the Brownian motion and the solution can be simply rewritten in terms of a harmonic measure, which measures the probability of the Brownian paths hitting a given area on the boundary surface,

$$u(\mathbf{x}) = E^x(\phi(X_{\tau_\Omega})) = \int_{\partial\Omega} \phi(\mathbf{y}) d\mu_\Omega^x, \quad (1.8)$$

where

$$\mu_\Omega^x(F) = P^x\{\omega | X_{\tau_\Omega}(\omega) \in F, X_0(\omega) = \mathbf{x}\}, \quad F \subset \partial\Omega, \quad \mathbf{x} \in \Omega. \quad (1.9)$$

The harmonic measure can be shown to be related to the Green's function  $g(\mathbf{x}, \mathbf{y})$  of the Laplace equation in the domain  $\Omega$  with a homogeneous boundary condition, i.e.,

$$\begin{aligned} -\Delta g(\mathbf{x}, \mathbf{y}) &= \delta(\mathbf{x} - \mathbf{y}), \quad \mathbf{x} \in \Omega, \\ g(\mathbf{x}, \mathbf{y})|_{\mathbf{x} \in \partial\Omega} &= 0. \end{aligned} \quad (1.10)$$

By comparing (1.8) with the following integral representation of the solution of the Laplace equation with the Green's function  $g(\mathbf{x}, \mathbf{y})$ ,

$$u(\mathbf{x}) = - \int_{\partial\Omega} \phi(\mathbf{y}) \frac{\partial g(\mathbf{x}, \mathbf{y})}{\partial \mathbf{n}_y} ds_y, \quad (1.11)$$

we conclude that the hitting probability, now denoted as  $p(\mathbf{x}, \mathbf{y}) ds_y = \mu_\Omega^x([\mathbf{y}, \mathbf{y} + ds_y])$ , has the following connection to the Green's function [10],

$$p(\mathbf{x}, \mathbf{y}) = - \frac{\partial g(\mathbf{x}, \mathbf{y})}{\partial \mathbf{n}_y}. \quad (1.12)$$

Therefore, if the domain is a ball centered at  $\mathbf{x}$  where a path starts, we have a uniform probability for the path to hit the surface of the ball. This fact will be a key factor in the design of random walk on spheres (WOS), which allows us to describe the Brownian motion and its exit location without explicitly finding its trajectory. Instead, a sequence of walks or jumps over spheres will allow the Brownian path hitting the boundary  $\partial\Omega$  (for practical purpose, within an absorption  $\varepsilon$ -shell as proposed in [21]). Specifically, as indicated by (1.12), the probability of a Brownian path hitting on a spherical surface is given exactly by the normal derivative of the Green's function of the sphere (with homogeneous boundary condition). Therefore, if we draw a ball centered at the starting point  $\mathbf{x}$  of a Brownian path, it will hit the spherical surface with a uniform probability as long as the ball does not intersect with the domain boundary  $\partial\Omega$ . So, we can make a jump for the Brownian particle to  $\mathbf{x}_1$ , sampled with a uniform distribution on the spherical surface. Next, a second ball now centered at  $\mathbf{x}_1$  will be drawn, not intersecting with the domain

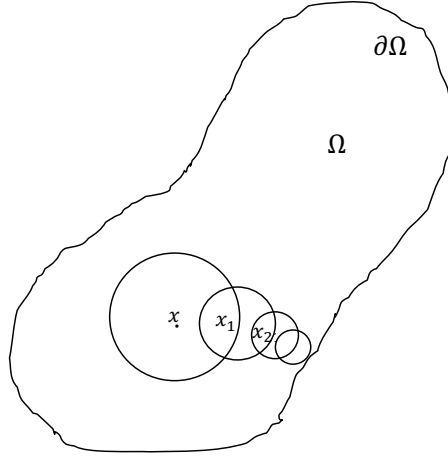


FIG. 1.1. WOS sampling of Brownian pathes

boundary  $\partial\Omega$ , the Brownian particle can make a second jump to  $\mathbf{x}_2$  on the surface of the second ball. This procedure (as illustrated in Fig 1.1, termed as WOS) [22][14][23], is repeated until it hits the boundary of  $\Omega$  (within the  $\varepsilon$ -shell of absorption) where it is denoted as  $\mathbf{x}_{\tau_\Omega}$  and the value of the boundary data  $\phi(\mathbf{x}_{\tau_\Omega})$  will be recorded and eventually all such data will be used to compute the expectation in (1.8).

In real applications, due to the relation between the Green's function  $g(\mathbf{x}, \mathbf{y})$  of a domain and the hitting probability, Green's Function First Passage (GFFP) methods for shapes other than spheres such as rectangles in softwares including QuickCap [8][9] have been used to find capacitances of conductors in interconnect layouts, which are generally of rectangular shapes.

The Feynman-Kac formula allows a local solution of the PDE, and fast sampling techniques of the diffusion pathes with the WOS methods are available for simple PDEs such as Laplace or modified Helmholtz equations. However, it is impractical to use the probabilistic formula to find the solution of these PDEs in whole space as too much sampling will be needed. In this paper, we will propose a hybrid method for computing the DtN mapping by combining the probabilistic Feynman-Kac formula and a deterministic local integral equation over domain boundary  $\partial\Omega$ . The hybrid method will allow us to get the Neumann data efficiently over a local patch of the domain boundary, which will result in a simple parallel method for solving the complete potential problems in general 3-D domains.

We will present the work in the following stages. Firstly, we will review a last passage method in [14] which calculates the Neumann data (charge distribution) *at one single point* over a flat surface when the Dirichlet data is a constant. Even though this is a very limited case for the DtN problem, it demonstrates some key issues and difficulties in how to use the Feynman-Kac

formula and the WOS in finding the Neumann data. Secondly, we will present our hybrid method, which allows the calculation of Neumann data for a general Dirichlet data on the flat surface. Thirdly, we extend the hybrid method to calculate the Neumann data over *a patch* of the boundary for arbitrary Dirichlet data and curved boundary. Numerical tests will be presented to show the accuracy and potential of the proposed methods. Finally, conclusion and discussions for open research issues and parallel aspect of the proposed method will be given.

## 2. Finding the Neumann data at one point over a flat boundary.

**2.1. Review of a last-passage algorithm for charge density.** In this subsection, we will review the last-passage Monte Carlo algorithm proposed in [14] for charge density, namely the Neumann data, at one point on a flat conducting surface.

For a flat portion of the boundary  $\partial\Omega$  of a domain  $\Omega = \{z < 0\}$  in the 3-D space held at a constant potential, we like to compute the charge density at a point  $\mathbf{x} \in \partial\Omega$ . In the last-passage method, a hemisphere is constructed with a radius  $a$  centered at  $\mathbf{x}$  as shown in Fig. 2.1 The upper hemispherical surface outside  $\Omega$  is denoted as  $\Gamma$  and the 2-D disk of radius  $a$  centered at  $\mathbf{x}$  from the intersection of the hemisphere and the conducting boundary  $\partial\Omega$  is denoted as

$$S_a \equiv S_a(\mathbf{x}). \quad (2.1)$$

From the discussion in Section 1 on the equivalence between the electrostatic potential and diffusion problems, the quantity  $v(\mathbf{x}) \equiv 1 - u(\mathbf{x} + \varepsilon)$  can be interpreted as the average value of  $v = 0$  on disk  $S_a$ , i.e.,

$$v(\mathbf{x}) = 0, \quad \mathbf{x} \in S_a \quad (2.2)$$

and  $v = 1$  at infinite (or on a infinitely large sphere). Therefore, we have the following probabilistic expression for  $v(\mathbf{x} + \varepsilon)$ , also viewed as the probability of a Brownian particle near the conducting surface  $\partial\Omega$  starting at  $\mathbf{x} + \varepsilon$  diffusing to infinity without ever coming back to the conducting surface [14][22]:

$$v(\mathbf{x} + \varepsilon) \equiv 1 - u(\mathbf{x} + \varepsilon) = - \int_{\Gamma} \widehat{g}(\mathbf{x} + \varepsilon, \mathbf{y}) p_{y\infty} ds_y, \quad (2.3)$$

where  $p_{y\infty}$  is the probability of a Brownian particle starting at  $\mathbf{y}$  and diffusing to infinity without ever coming back to the conducting surface  $\partial\Omega$ , thus,  $p_{y\infty} = 0$  if  $\mathbf{y} \in S_a$ . In (2.3), the integral over  $\Gamma$  expresses the Markov property of the diffusing particles from  $\mathbf{x} + \varepsilon$  to the infinity with an intermediate stop on  $\Gamma$ . Specifically,  $\widehat{g}(\mathbf{x} + \varepsilon, \mathbf{y})$  gives the probability of a Brownian particle starting from  $\mathbf{x} + \varepsilon$  hitting the boundary of  $\Gamma$ , which is given by (1.12) via a homogeneous Green's function for the hemisphere over  $S_a$ , namely,

$$\widehat{g}(\mathbf{x} + \varepsilon, y) = \frac{\partial g}{\partial \mathbf{n}_y}(\mathbf{x} + \varepsilon, \mathbf{y}), \quad (2.4)$$

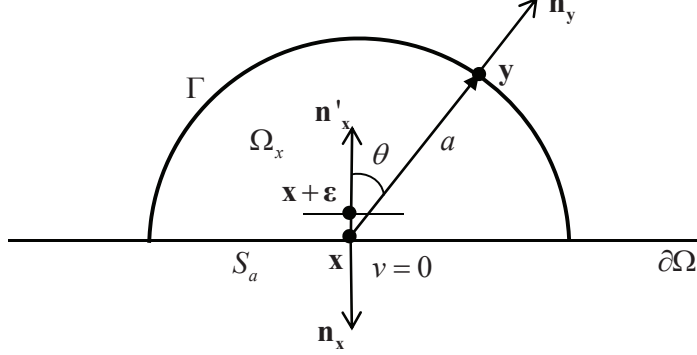


FIG. 2.1. Last passage for finding the Neumann data at one point

and  $g(\mathbf{x} + \varepsilon, y)$  is defined in (1.10) for the hemisphere, whose analytical form can be obtained by an image method with respect to spherical surface first, then to the half plane  $z = 0$ , resulting in the use of 3 images. Specifically, we have

$$g(\mathbf{x}, \mathbf{x}_s) = \frac{1}{4\pi} \frac{1}{|\mathbf{x} - \mathbf{x}_s|} + \frac{1}{4\pi} \frac{q_k}{|\mathbf{x} - \mathbf{x}_k|} + \frac{1}{4\pi} \frac{q_{\bar{s}}}{|\mathbf{x} - \mathbf{x}_{\bar{s}}|} + \frac{1}{4\pi} \frac{q_{\bar{k}}}{|\mathbf{x} - \mathbf{x}_{\bar{k}}|}, \quad (2.5)$$

where in spherical coordinates the source location is  $\mathbf{x}_s = (\rho_s, \theta_s, \phi_s)$ , the Kelvin image location with respect to the sphere is  $\mathbf{x}_k = (a^2/\rho_s, \theta_s, \phi_s)$ , and their mirror image locations with respect to the plane  $z = 0$  are  $\mathbf{x}_{\bar{s}} = (\rho_s, \pi - \theta_s, \phi_s)$ ,  $\mathbf{x}_{\bar{k}} = (a^2/\rho_s, \pi - \theta_s, \phi_s)$ , respectively. Meanwhile, the corresponding charges are  $q_k = -a/\rho_s$ ,  $q_{\bar{s}} = -1$ , and  $q_{\bar{k}} = a/\rho_s$ , respectively.

Now, to get the charge distribution  $\sigma_s$  (normal derivative), we use the relation in (1.1), we have

$$\sigma_s = -\lim_{\varepsilon \rightarrow 0} \mathbf{n}_{x+\varepsilon} \cdot \mathbf{E}(\mathbf{x} + \varepsilon) = \lim_{\varepsilon \rightarrow 0} \frac{\partial u(\mathbf{x} + \varepsilon)}{\partial \mathbf{n}_x} = \frac{\partial u(\mathbf{x})}{\partial \mathbf{n}_x}, \quad (2.6)$$

and

$$\frac{\partial u(\mathbf{x})}{\partial \mathbf{n}_x} = \int_{\Gamma} h(\mathbf{x} + \varepsilon, \mathbf{y}) p_{y\infty} ds_y \equiv \Sigma_{LP}, \quad (2.7)$$

where a shorthand  $\Sigma_{LP}$  is introduced for the integral over  $\Gamma$  for latter use, and

$$h(\mathbf{x}, \mathbf{y}) = \frac{\partial^2}{\partial \mathbf{n}_y \partial \mathbf{n}_x} g(\mathbf{x} + \varepsilon, \mathbf{y}). \quad (2.8)$$

The weight function  $h(\mathbf{x}, \mathbf{y})$  can be analytically computed for the hemisphere

$$h(\mathbf{x}, \mathbf{y}) = \frac{3}{2\pi} \frac{\cos \theta}{a^3}, \quad (2.9)$$

where  $\theta$  is the angle between the two normal vectors  $\mathbf{n}'_x$  and  $\mathbf{n}_y$  on the boundary  $\Gamma$  as shown in Fig. 2.1.

Next, we only need to compute  $p_{y\infty}$  which is the probability of a Brownian particle starting from  $\mathbf{y} \in \Gamma$  and diffuse to infinity without ever returning to the conductor surface  $\partial\Omega$ . Due to the homogeneity of the Brownian motion in the external domain  $\Omega^c = \{z > 0\}$ , the WOS in Section 1 can be used to calculate this probability. The integral in (2.7) over  $\Gamma$  could be approximated by a Gauss quadrature as both  $h(\mathbf{x}, \mathbf{y})$  and  $p_{y\infty}$  can be considered as smooth functions of  $\mathbf{y} \in \Gamma$ . Nonetheless, in [14], the integral  $\Sigma_{\text{LP}}$  is computed by first distributing  $N$  particles at locations over  $\Gamma$  based on a distribution density derived from (2.9), and then starting a Brownian diffusion path from each of those locations. The number of paths which will diffuse to infinity (in practice, when it hits a very large ball) is recorded as  $N_{\text{inf}}$ , then, we have the following estimate

$$\Sigma_{\text{LP}} \simeq \frac{3}{2a} \frac{N_{\text{inf}}}{N}. \quad (2.10)$$

The key equation in the last-passage algorithm is (2.7), which is based on (2.3) provided that the potential solution  $v(\mathbf{x}) = 0, \mathbf{x} \in S_a$  on the conductor surface as indicated in (2.2). Therefore, for general non-constant Dirichlet boundary data, the last passage method will not be applicable. In fact, the charge density at  $\mathbf{x}$  will be influenced by potential value on all domain boundary.

**2.2. BIE-WOS Method: Combining a BIE and the Monte Carlo WOS method.** For the last-passage method discussed above, the algorithm (2.7) is obtained by the isomorphism between the electrostatic potential and diffusion problems. The limitation of the last passage method is that it is only applicable to the situation of constant Dirichlet data and a flat boundary. In this section, we will adopt a different approach based on a boundary integral equation (BIE) representation of the charge density (the Neumann data) on the surface at a given point using potential over a small hemisphere, the latter can be then computed by the random WOS method. As a result, this new approach, a hybrid method of deterministic and random approaches, will be able to handle general variable Dirichlet boundary data, and later in Section 3 also be extended to curved boundaries.

Let us denote by  $\Omega_x$  the domain formed by the hemisphere of radius  $a$  centered at  $\mathbf{x}$  over the flat boundary boundary  $S_a$  as in Fig. 2.1, by applying the integral representation (1.3) of Laplace equation with the afore-mentioned Green's function  $g(\mathbf{x}, \mathbf{y})$  in (2.5) for the domain  $\Omega_x$  with a homogeneous Dirichlet boundary condition. Due to the zero boundary value of the Green's function  $g(\mathbf{x}, \mathbf{y})$ , we have

$$u(\mathbf{x}') = - \int_{\Gamma \cup S_a} \frac{\partial g(\mathbf{x}, \mathbf{y})}{\partial \mathbf{n}_y} u(\mathbf{y}) ds, \quad \mathbf{x}' \in \Omega_x, \quad (2.11)$$



where  $\Gamma$  again is the surface of the upper hemisphere and  $S_a$  is the disk of radius  $a$  centered at  $\mathbf{x}$ . In order to obtain the normal derivative of  $u$  at  $\mathbf{x}$ , we simply take the derivative with respect to  $\mathbf{x}'$  along the direction  $\mathbf{n}_{\mathbf{x}}$  as  $\mathbf{x}'$  approaches  $\mathbf{x}$  and obtain the following representations involving a hyper-singular kernel,

$$\frac{\partial}{\partial \mathbf{n}_{\mathbf{x}}} u(\mathbf{x}) = - \lim_{\mathbf{x}' \rightarrow \mathbf{x}} \int_{\Gamma \cup S_a} \frac{\partial^2 g(\mathbf{x}', \mathbf{y})}{\partial \mathbf{n}_{\mathbf{y}} \partial \mathbf{n}_{\mathbf{x}}} u(\mathbf{y}) ds, \quad \mathbf{x} \in S_a. \quad (2.12)$$

The integral expression for  $\frac{\partial}{\partial \mathbf{n}_{\mathbf{x}}} u(\mathbf{x})$  involves two integrals, one regular integration over the upper hemisphere  $\Gamma$  denoted as

$$\Sigma_1 = - \int_{\Gamma} \frac{\partial^2 g(\mathbf{x}, \mathbf{y})}{\partial \mathbf{n}_{\mathbf{y}} \partial \mathbf{n}_{\mathbf{x}}} u(\mathbf{y}) ds_y = - \int_{\Gamma} \left( \frac{3}{2\pi} \frac{\cos \theta}{a^3} \right) u(\mathbf{y}) ds_y, \quad (2.13)$$

where (2.9) has been used in the second equality, and another hyper-singular integral over the disk  $S_a$  denoted as

$$\Sigma_2 = - \lim_{\mathbf{x}' \rightarrow \mathbf{x}} \int_{S_a} \frac{\partial^2 g(\mathbf{x}', \mathbf{y})}{\partial \mathbf{n}_{\mathbf{y}} \partial \mathbf{n}_{\mathbf{x}}} u(\mathbf{y}) ds_y, \quad (2.14)$$

and we have

$$\frac{\partial}{\partial \mathbf{n}_{\mathbf{x}}} u(\mathbf{x}) = \Sigma_1 + \Sigma_2. \quad (2.15)$$

Equation (2.15) will be the starting point for the proposed hybrid method. In computing the integral  $\Sigma_1$ , say by a Gauss quadrature over the hemisphere surface, we will need the potential solution  $u(\mathbf{y})$  for  $\mathbf{y} \in \Gamma$  and this solution will be readily computed with the Feynman-Kac formula (1.8) with the WOS as the sampling technique for the Brownian paths. On the other hand, the singular integral  $\Sigma_2$ , with appropriate treatment of the hyper-singularities to be described in detail in the numerical test section, can be calculated directly with the given Dirichlet boundary data  $u(\mathbf{y}), \mathbf{y} \in S_a$ . Therefore, an algorithm using (2.12) involves the hybridization of a random walk on spheres (WOS) and a deterministic boundary integral equation (BIE), which is termed the *BIE-WOS method*.

**Remark:** In comparing the last-passage method (2.7) and the BIE-WOS method (2.15), the former uses the relation between the Brownian motion of diffusive particles and electric potential from charges on a conducting surface to arrive at an expression for the surface charge density based on (2.7). The BIE-WOS uses an hyper-singular boundary integral equation to get a similar expression in (2.15), which has an additional contribution from the variable potential on the charged surfaces (the integral term  $\Sigma_2$ ). Both methods use WOS for particles starting on the hemisphere, however, at different locations. The last-passage method proposed in ([14]) initiates particles walk starting from

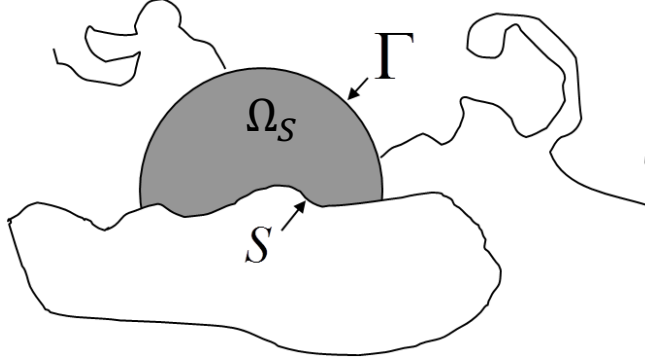


FIG. 3.1. Setup of the BIE-WOS method for finding Neumann data on a patch  $S \subset \partial\Omega$ .

positions all over the hemisphere sampled using a probability given by (2.9) while BIE-WOS initiates many particle walks starting from selected Gauss quadrature points (up to  $30 \times 30$  in our test problems). Numerical results will show that for problems suitable for both methods, the total number of particle walk paths and the accuracy and computational costs are comparable (refer to Test 4 in Section 4.1.3).

**3. Finding Neumann data over a patch of general boundary.** In this section, we will extend the BIE-WOS of last section to the case of general Dirichlet boundary data and curved domain boundary. To achieve this goal, we will superimpose an hemisphere over any selected portion of the boundary  $\partial\Omega$  and denote the intersection portion of the domain boundary by  $S$  and the surface of the hemisphere outside the domain  $\Omega$  still by  $\Gamma$  and the region bounded by  $S$  and  $\Gamma$  is denoted as  $\Omega_S$  (see Fig. 3.1). Now let  $G(\mathbf{x}, \mathbf{y})$  be the Green's function of a *whole sphere* with an homogeneous boundary condition and  $G(\mathbf{x}, \mathbf{y})$  can be easily obtained by one Kelvin image charge as discussed before. Then, the integral representation (1.3) can be applied to the boundary of the domain  $\Omega_S$  to yield the following identity

$$u(\mathbf{x}) = - \int_{\Gamma} \frac{\partial G(\mathbf{x}, \mathbf{y})}{\partial \mathbf{n}_y} u(\mathbf{y}) ds_y + \int_S \left[ - \frac{\partial G(\mathbf{x}, \mathbf{y})}{\partial \mathbf{n}_y} u(\mathbf{y}) + G(\mathbf{x}, \mathbf{y}) \frac{\partial u(\mathbf{y})}{\partial \mathbf{n}_y} \right] ds_y, \quad \mathbf{x} \in \Omega_S \quad (3.1)$$

It should be noted that the integral over  $\Gamma$  only involves the normal derivative of the Green's function as  $G$  vanishes on  $\Gamma$  by construction. As a result, only solution  $u(\mathbf{y})$  is needed on  $\Gamma$  while both  $u(\mathbf{y})$  and the normal derivative  $\frac{\partial u(\mathbf{y})}{\partial \mathbf{n}}$  appear in the integral over  $S$ . As before, the solution  $u(\mathbf{y})$  over  $\Gamma$  will be computed with the Feynman-Kac formula (1.8) with WOS and then the Neumann data over  $S$  can be solved from the following integral equation,

$$K \left[ \frac{\partial u}{\partial \mathbf{n}} \right] (\mathbf{x}) = b(\mathbf{x}), \quad \mathbf{x} \in S, \quad (3.2)$$

where

$$K \left[ \frac{\partial u}{\partial \mathbf{n}} \right] \equiv \int_S G(\mathbf{x}, \mathbf{y}) \frac{\partial u(\mathbf{y})}{\partial \mathbf{n}_{\mathbf{y}}} ds_{\mathbf{y}}, \quad (3.3)$$

and

$$b(\mathbf{x}) \equiv \left( \frac{u(\mathbf{x})}{2} + \text{p.v.} \int_S \frac{\partial G(\mathbf{x}, \mathbf{y})}{\partial \mathbf{n}_{\mathbf{y}}} u(\mathbf{y}) ds_{\mathbf{y}} \right) + \int_{\Gamma} \frac{\partial G(\mathbf{x}, \mathbf{y})}{\partial \mathbf{n}_{\mathbf{y}}} u(\mathbf{y}) ds_{\mathbf{y}}. \quad (3.4)$$

Integral equation (3.2) is of the first kind which is ill-conditioned and may cause numerical difficulties especially when the algebraic system from discretization becomes large. When that happens, a well-conditioned second kind of integral equation can be obtained by taking normal derivative of (3.1), resulting in the following identity for  $\mathbf{x} \in \Omega_S$

$$\frac{\partial}{\partial \mathbf{n}_{\mathbf{x}}} u(\mathbf{x}) = - \int_{\Gamma} \frac{\partial^2 G(\mathbf{x}, \mathbf{y})}{\partial \mathbf{n}_{\mathbf{y}} \partial \mathbf{n}_{\mathbf{x}}} u(\mathbf{y}) ds_{\mathbf{y}} + \int_S \left[ - \frac{\partial^2 G(\mathbf{x}, \mathbf{y})}{\partial \mathbf{n}_{\mathbf{y}} \partial \mathbf{n}_{\mathbf{x}}} u(\mathbf{y}) + \frac{\partial G(\mathbf{x}, \mathbf{y})}{\partial \mathbf{n}_{\mathbf{x}}} \frac{\partial u(\mathbf{y})}{\partial \mathbf{n}_{\mathbf{y}}} \right] ds_{\mathbf{y}}. \quad (3.5)$$

Let  $\mathbf{x}$  approaching the boundary  $S$ , we obtain the following second kind integral equation

$$\left( \frac{1}{2} I - D \right) \left[ \frac{\partial u}{\partial \mathbf{n}} \right] (\mathbf{x}) = b(\mathbf{x}), \quad \mathbf{x} \in S, \quad (3.6)$$

where the integral operator of a double layer potential

$$D \left[ \frac{\partial u}{\partial \mathbf{n}} \right] (\mathbf{x}) \equiv \int_S \frac{\partial G(\mathbf{x}, \mathbf{y})}{\partial \mathbf{n}_{\mathbf{x}}} \frac{\partial u(\mathbf{y})}{\partial \mathbf{n}_{\mathbf{y}}} ds_{\mathbf{y}}, \quad (3.7)$$

and

$$b(\mathbf{x}) \equiv - \int_{\Gamma} \frac{\partial^2 G(\mathbf{x}, \mathbf{y})}{\partial \mathbf{n}_{\mathbf{y}} \partial \mathbf{n}_{\mathbf{x}}} u(\mathbf{y}) ds_{\mathbf{y}} - \text{p.f.} \int_S \frac{\partial^2 G(\mathbf{x}, \mathbf{y})}{\partial \mathbf{n}_{\mathbf{y}} \partial \mathbf{n}_{\mathbf{x}}} u(\mathbf{y}) ds_{\mathbf{y}}, \quad \mathbf{x} \in S, \quad (3.8)$$

and p.f. denotes the Hadamard finite part limit for the hyper-singular integral, which can be handled by a regularization technique.

**BIE-WOS Algorithm:** The BIE-WOS method for the Neumann data over a patch  $S$  will consist of two steps:

- Step 1: Apply the Feynman-Kac formula (1.8) with the WOS sample technique to compute the potential solution at Gauss points  $\mathbf{y}_{i,j} \in \Gamma$ ,  $u(\mathbf{y}_{i,j})$ . Compute the right hand side function  $b(\mathbf{x})$  in (3.4) or (3.8) by some Gauss quadratures.
- Step 2: Solve the BIE (3.2) or (3.6) with a collocation method for the Neumann data  $\frac{\partial u}{\partial \mathbf{n}}$  over  $S$ .

**4. Numerical Results.** In this section, we will present a series of numerical tests to demonstrate the accuracy and efficiency of the proposed BIE-WOS method for finding the Neumann data at a single point on a flat boundary and on a patch over a curved boundary.

#### 4.1. Finding Neumann data at one point on a flat boundary.

**4.1.1. Regularization of hyper-singular integrals.** First, let us present a regularization method using simple solution of the Laplace equation [16] to compute the hyper-singular integral in (2.14) and (3.8). First, with some simple calculations, the term  $\Sigma_2$  of (2.14) is found to be a Hadamard finite part limit of the following hyper-singular integral:

$$\Sigma_2 = -\lim_{\mathbf{x}' \rightarrow \mathbf{x}} \int_{S_a} \frac{\partial^2 g(\mathbf{x}', \mathbf{y})}{\partial \mathbf{n}_y \partial \mathbf{n}_x} u(\mathbf{y}) ds_y = -\text{p.f.} \int_{S_a} \frac{1}{2\pi} \left( \frac{1}{\rho^3} - \frac{1}{a^3} \right) u(\mathbf{y}) ds_y, \quad (4.1)$$

where  $\rho = |\mathbf{x} - \mathbf{y}|$ ,  $\mathbf{x}, \mathbf{y} \in S_a$ . The finite part (p.f.) limit of Hadamard type is defined by removing a divergent part in the process of defining a principal value (i.e. by removing a small patch of size  $\varepsilon$  centered at  $\mathbf{x}$  and then let  $\varepsilon$  approaching zero). For the Laplace equation considered here, we can regularize this hyper-singularity by invoking an integral identity for the special solution  $u \equiv \phi(\mathbf{x})$ ,  $\mathbf{x}$  is fixed, namely, the integral identity (2.12) applied to this constant solution results in

$$0 = -\int_{\Gamma} \frac{\partial^2 g(\mathbf{x}, \mathbf{y})}{\partial \mathbf{n}_y \partial \mathbf{n}_x} \phi(\mathbf{x}) ds - \lim_{\mathbf{x}' \rightarrow \mathbf{x}} \int_{S_a} \frac{\partial^2 g(\mathbf{x}', \mathbf{y})}{\partial \mathbf{n}_y \partial \mathbf{n}_x} \phi(\mathbf{x}) ds, \quad \mathbf{x} \in S. \quad (4.2)$$

Subtracting (4.2) from (2.15), we have a modified formula for the Neumann data as

$$\frac{\partial}{\partial n_x} u(\mathbf{x}) = \Sigma'_1 + \Sigma'_2, \quad \mathbf{x} \in S, \quad (4.3)$$

where  $\Sigma'_1$  and  $\Sigma'_2$  are now regularized versions of  $\Sigma_1$  and  $\Sigma_2$  in (2.13) and (2.14), respectively, i.e.,

$$\Sigma'_1 = -\int_{\Gamma} \frac{\partial^2 g(\mathbf{x}, \mathbf{y})}{\partial \mathbf{n}_y \partial \mathbf{n}_x} (u(\mathbf{y}) - \phi(\mathbf{x})) ds_y, \quad (4.4)$$

and

$$\begin{aligned} \Sigma'_2 &= -\lim_{\mathbf{x}' \rightarrow \mathbf{x}} \int_{S_a} \frac{\partial^2 g(\mathbf{x}', \mathbf{y})}{\partial \mathbf{n}_y \partial \mathbf{n}_x} (u(\mathbf{y}) - \phi(\mathbf{x})) ds_y \\ &= -\lim_{\mathbf{x}' \rightarrow \mathbf{x}} \int_{S_a} \frac{1}{2\pi} \left( \frac{1}{r^3} - \frac{1}{a^3} \right) (\phi(\mathbf{y}) - \phi(\mathbf{x})) ds_y, \end{aligned} \quad (4.5)$$

where  $\mathbf{x}' = \mathbf{x} + (0, 0, \varepsilon)$ ,  $r = \sqrt{\rho^2 + \varepsilon^2}$ ,  $\rho = |\mathbf{x} - \mathbf{y}|$ ,  $\mathbf{x}, \mathbf{y} \in S_a$ . Moreover, the boundary condition  $u(\mathbf{y}) = \phi(\mathbf{y})$ ,  $\mathbf{y} \in S_a$  has been invoked in (4.5).

Compared with (4.1), the singularity in the integral  $\Sigma'_2$  in (4.5) has been weakened by the factor  $(\phi(\mathbf{y}) - \phi(\mathbf{x}))$ , which vanishes at  $\mathbf{x}$ , and  $\Sigma'_2$  will be evaluated by a Gauss quadrature. Let us only consider the integral involving the singular term  $\frac{1}{r^3}$  in (4.5), which is denoted by  $\Sigma_2^*$ , i.e.,

$$\Sigma_2^* = -\frac{1}{2\pi} \lim_{\mathbf{x}' \rightarrow \mathbf{x}} \int_{S_x} \frac{1}{r^3} (\phi(\mathbf{y}) - \phi(\mathbf{x})) ds_y. \quad (4.6)$$

Consider a circular patch  $\Lambda_\delta$  of radius  $\delta$  centered at  $\mathbf{x}$ , and then  $\Sigma_2^*$  can be split further into two integrals as follows

$$\begin{aligned} \Sigma_2^* &= -\frac{1}{2\pi} \int_{S_a \setminus \Lambda_\delta} \frac{1}{\rho^3} (\phi(\mathbf{y}) - \phi(\mathbf{x})) ds_y \\ &\quad - \frac{1}{2\pi} \lim_{\mathbf{x}' \rightarrow \mathbf{x}} \int_{\Lambda_\delta} \frac{1}{r^3} (\phi(\mathbf{y}) - \phi(\mathbf{x})) ds_y \\ &= -\frac{1}{2\pi} \int_{S_a \setminus \Lambda_\delta} \frac{1}{\rho^3} (\phi(\mathbf{y}) - \phi(\mathbf{x})) ds_y + \Delta. \end{aligned} \quad (4.7)$$

To estimate the term  $\Delta$ , we apply a Taylor expansion of the boundary data  $\phi(\mathbf{y})$  at  $\mathbf{x}$

$$\phi(\mathbf{y}) - \phi(\mathbf{x}) = \nabla \phi(\mathbf{x}) \cdot \boldsymbol{\rho} + O(\rho^2), \quad (4.8)$$

then, we obtain

$$\begin{aligned} \Delta &= -\frac{\nabla \phi(\mathbf{x}) \cdot}{2\pi} \lim_{\mathbf{x}' \rightarrow \mathbf{x}} \int_{\Lambda_\delta} \frac{\boldsymbol{\rho}}{r^3} ds_y + \frac{1}{2\pi} \int_{\Lambda_\delta} \frac{O(\rho^2)}{r^3} ds_y \\ &= -\frac{\nabla \phi(\mathbf{x}) \cdot}{2\pi} \lim_{\mathbf{x}' \rightarrow \mathbf{x}} \int_0^\delta \int_0^{2\pi} \frac{\rho(\cos \theta, \sin \theta)}{(\rho^2 + \varepsilon^2)^{3/2}} \rho d\theta d\rho \\ &\quad + \lim_{\mathbf{x}' \rightarrow \mathbf{x}} \int_0^\delta \frac{O(\rho^2)}{(\rho^2 + \varepsilon^2)^{3/2}} \rho d\rho \\ &= 0 + \lim_{\mathbf{x}' \rightarrow \mathbf{x}} \int_0^\delta \frac{O(\rho^3)}{(\rho^2 + \varepsilon^2)^{3/2}} d\rho. \end{aligned} \quad (4.9)$$

Now for all positive  $\varepsilon > 0$ , we have

$$\frac{\rho^3}{(\rho^2 + \varepsilon^2)^{3/2}} \leq 1, \quad (4.10)$$

as a result, the following estimate of the term  $\Delta$  holds

$$\Delta = O(\delta). \quad (4.11)$$

Finally, the regularized integral  $\Sigma_2^*$  will be approximated by the integral over  $S_a \setminus \Lambda_\delta$  with an accuracy of  $O(\delta)$  and a Gauss quadrature formula over the ring shaped region  $S_a \setminus \Lambda_\delta$ :

$$\Sigma_2^* = -\frac{1}{2\pi} \int_{S_a \setminus \Lambda_\delta} \frac{1}{\rho^3} (\phi(\mathbf{y}) - \phi(\mathbf{x})) ds_y + O(\delta). \quad (4.12)$$

#### 4.1.2. Gauss integrals over the hemisphere $\Gamma$ and $S_a \setminus \Lambda_\delta$ and WOS.

To compute the integral  $\Sigma'_1$ , we use  $N_{g1} \times N_{g1}$  Gauss points over the hemisphere surface  $\Gamma$

$$\Sigma'_1 \simeq - \sum_{i,j=1}^{N_{g1}} \omega_i \omega_j \frac{\pi^2}{4} (a^2 \sin \theta_i) \frac{3}{2a} \left( \frac{\cos \theta_i}{\pi a^2} \right) (u(\mathbf{y}_{i,j}) - \phi(\mathbf{x})), \quad (4.13)$$

where

$$\theta_i = \frac{\pi}{4}(\xi_i + 1), \varphi_j = \pi(\xi_j + 1), \mathbf{y}_{i,j} = (a, \theta_i, \varphi_j), \quad (4.14)$$

and  $\omega_i$  and  $\xi_i, 1 \leq i \leq N_{g1}$  are the Gauss quadrature weights and locations, respectively.  $\frac{\pi^2}{4}(a^2 \sin \theta_i)$  is the surface element in the spherical coordinates.

Now, each of the solution value  $u(\mathbf{y}_{i,j})$ ,  $\mathbf{y}_{i,j} \in \Gamma$  will be obtained by the Feynman-Kac formula (1.8) with  $N_{path}$  Brownian particles all starting from  $\mathbf{y}_{i,j}$ , namely

$$u(\mathbf{y}_{i,j}) \simeq \frac{1}{N_{path}} \sum_{path \ k=1}^{N_{path}} \phi(\mathbf{e}_k), \quad (4.15)$$

where  $\mathbf{e}_k$  is the location on  $\partial\Omega$  where a path terminates.

The total number  $N_{path-bie-wos}$  of Brownian particles needed in the BIE-WOS method will be

$$N_{path-bie-wos} = N_{g1} \times N_{g1} \times N_{path}. \quad (4.16)$$

Next, the integral  $\Sigma_2^*$  in (4.12) will be computed with another  $N_{g2} \times N_{g2}$  Gauss quadrature over the ring shaped region  $S_a \setminus \Lambda_\delta$  with an error of  $O(\delta)$  in addition to the error from the Gauss quadrature.

**4.1.3. Numerical tests.** In this section, we will present several numerical tests to demonstrate the accuracy and efficiency of the proposed BIE-WOS for finding the Neumann data at a given point over a flat boundary for general Dirichlet boundary data. For comparison, we also implement the last-passage Monte Carlo method in [14]. For accuracy comparison, the charge density is calculated with the FastCap, an open-source code developed in MIT [24] for 3-D capacitance extraction tool in industry and academia. The Fastcap is an indirect BEM, accelerated by the fast multipole method (FMM), and its linear system is solved by a conjugate gradient method. For the case of complex potentials on the surfaces, we also implemented a direct BEM (DBEM) [29].

#### • Test 1- Charge densities on a planar interface between two dielectric half spaces

As shown in Fig. 4.1, the whole space is divided by a planar interface between the two dielectric domains, and the dielectric constants are  $\epsilon_0$  and  $\epsilon_1$  in the upper and lower domain, respectively. A charge  $q$  is located at  $\mathbf{r}_s = (0, 0, -h)$  and then the potential in the upper space is given by

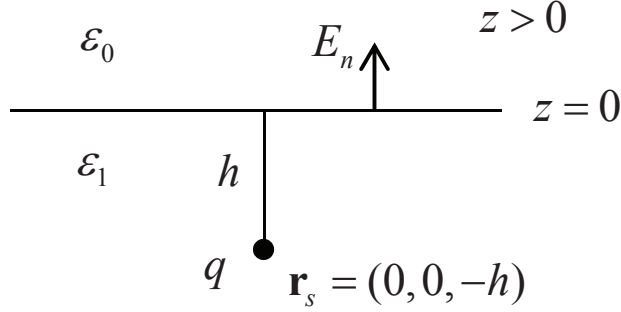


FIG. 4.1. *Potential above a half-space*

TABLE 4.1  
CHARGE DENSITY ON THE HALF PLANE INTERFACE WITH DIFFERENT RADIUS

| $a$ | Last-passage  |        | Bie-WOS     |             |                         |       | analytical<br>solution |
|-----|---------------|--------|-------------|-------------|-------------------------|-------|------------------------|
|     | $\Sigma_{LP}$ | err%   | $\Sigma'_1$ | $\Sigma'_2$ | $\Sigma'_1 + \Sigma'_2$ | err%  |                        |
| 0.1 | 0.698543      | -2.38  | 0.69884     | 0.018777    | 0.717612                | 0.29  | 0.71554                |
| 0.2 | 0.677996      | -5.25  | 0.67784     | 0.037515    | 0.715355                | -0.03 |                        |
| 0.5 | 0.622949      | -12.94 | 0.62146     | 0.093054    | 0.714517                | -0.14 |                        |
| 0.7 | 0.586721      | -18.00 | 0.58432     | 0.128971    | 0.713287                | -0.32 |                        |
| 1.0 | 0.534695      | -25.27 | 0.53659     | 0.179973    | 0.716562                | 0.14  |                        |

$$u(\mathbf{r}) = \frac{q'}{4\pi\epsilon_0} \frac{1}{|\mathbf{r} - \mathbf{r}_s|}, \quad q' = \frac{2\epsilon_0}{\epsilon_0 + \epsilon_1} q, \quad (4.17)$$

and  $u(\mathbf{r})$  satisfies the Laplace equation  $\nabla^2 u(\mathbf{r}) = 0, z > 0$  with a variable Dirichlet data on the boundary  $z = 0$ .

The charge density at the point  $\mathbf{x} = (0.5, 0, 0)$  by the last-passage method and BIE-WOS with various radius  $a$  of the hemisphere are listed in Table 4.1. In the last-passage method, the total number of the sampling paths  $N = 4 \times 10^5$ . In the BIE-WOS, the number of Gauss points  $N_{g1} \times N_{g1} = 20 \times 20$  for the hemisphere and  $N_{g2} \times N_{g2} = 20 \times 20$  for the integral on the 2-D disk  $S_a$ , and starting from each Gauss point on the hemisphere, the number of the sampling paths is  $N_{path} = 10^3$ . Therefore, the total number of paths for the BIE-WOS method is also  $4 \times 10^5$ . In both methods, the thickness of the absorption layer  $\epsilon$  for the WOS method is taken to be  $10^{-5}$ , and the step threshold for going to infinity  $N_{step} = 300$ .

From Table 4.1, we can see that when the radius becomes larger, the relative errors of the last-passage method grows and even up to  $-25.27\%$ . It shows that when the potential Dirichlet data on the disk  $S_a$  is not constant, the last-passage method is not applicable. The variable potential inside the

TABLE 4.2  
ACCURACY OF WITH AND

| $\delta/a$ | $\Sigma'_2$ calculated by $N_{g2} \times N_{g2}$ Gauss Quadrature |       |              |        |                |        |                |         |
|------------|-------------------------------------------------------------------|-------|--------------|--------|----------------|--------|----------------|---------|
|            | $4 \times 4$                                                      | err%  | $6 \times 6$ | err%   | $10 \times 10$ | err%   | $20 \times 20$ | err%    |
| $10^{-1}$  | 0.09659                                                           | 3.800 | 0.08983      | -3.462 | 0.08949        | -3.833 | 0.08949        | -3.8351 |
| $10^{-2}$  | 0.10042                                                           | 7.916 | 0.09306      | 0.001  | 0.09273        | -0.347 | 0.09273        | -0.3492 |
| $10^{-3}$  | 0.10083                                                           | 8.352 | 0.09335      | 0.314  | 0.09302        | -0.033 | 0.09302        | -0.0346 |
| $10^{-4}$  | 0.10087                                                           | 8.397 | 0.09337      | 0.345  | 0.09305        | -0.002 | 0.09305        | -0.0035 |
| $10^{-5}$  | 0.10087                                                           | 8.402 | 0.09338      | 0.348  | 0.09306        | 0.001  | 0.09305        | -0.0003 |
| $10^{-6}$  | 0.10087                                                           | 8.402 | 0.09338      | 0.348  | 0.09306        | 0.001  | 0.09305        |         |

disk  $S_a$  at the bottom of the hemisphere will influence the charge density at  $\mathbf{x}$  to be calculated. In contrast, the BIE-WOS includes such influences as shown in the results, and most importantly, it is independent of the radius  $a$ , for its maximal relative errors is less than 0.32% when the radius ranges from 0.1 to 1.0.

Table 4.2 lists the accuracy of the de-singularized  $\Sigma'_2$  in (4.12) with different values  $\delta$  and number of Gauss points  $N_{g2} \times N_{g2}$ , where the location of the sought-after density is at  $(0.5, 0, 0)$ . The result of  $N_{g2} \times N_{g2} = 20 \times 20$  with  $\delta/a = 10^{-6}$  is taken as the reference value for  $\Sigma'_2$ . Table 4.2 shows the convergence speed of  $\Sigma'_2$  as  $\delta/a$  goes to zero and number of Gauss points increases. It can be seen that when the number of the Gauss point is large enough, for example  $20 \times 20$ , the relative error is on the order of  $\delta/a$ , verifying the estimate in (4.12) .

• *Test 2: Four rectangle plates with a piecewise constant potential distribution*

A 3-D structure with four rectangle plates is depicted in Fig. 4.2, where the length, width and thickness of all four unit plates are  $1\text{m} \times 1\text{m} \times 0.01\text{m}$ . First, we set the potential of plate II to 1V and other three (I, III and IV) to 0V, and compute the charge density at the point  $A(-0.2273, 0.2273)$ . The results of all four methods are listed in Table 4.3, taking the results by the FastCap as the reference where each side of the plates is discretized into  $99 \times 99$  panels. The DBEM uses a discretization with  $11 \times 11$  panels on each side, its relative error is -0.46%.

Both last-passage method and BIE-WOS run with various radius  $a$  of the hemisphere, and the parameters are the same as in Test 1. In this case, the integral  $\Sigma'_2$  is related to the area of the intersecting area between the disk  $S_a$  and the plate I, III and IV, we just compute it directly by the *quad* function in Matlab, instead of Gauss quadratures.

Note that the potential on the boundary  $\partial\Omega$  here is piecewise constant. Therefore, in the last-passage method, charge density should be computed,



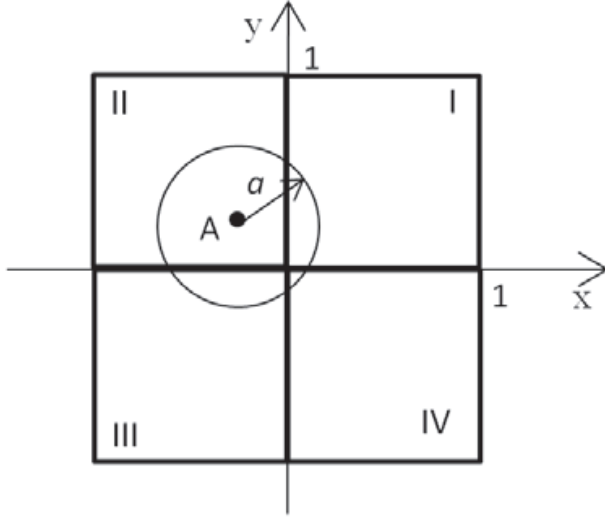


FIG. 4.2. Four plates at different potentials

TABLE 4.3  
CHARGE DENSITY OF A FOUR UNIT PLATES STRUCTURE WITH DIFFERENT RADIUS

| $a$    | Last passage  |        | BIE-WOS     |             |                         |       | DBEM    |       |
|--------|---------------|--------|-------------|-------------|-------------------------|-------|---------|-------|
|        | $\Sigma_{LP}$ | err%   | $\Sigma'_1$ | $\Sigma'_2$ | $\Sigma'_1 + \Sigma'_2$ | err%  | value   | err%  |
| 0.1    | 2.6084        | 0.05   | 2.6051      | 0           | 2.6051                  | -0.07 | 2.595   | -0.46 |
| 0.2    | 2.6026        | -0.17  | 2.6051      | 0           | 2.6051                  | -0.07 |         |       |
| 0.2273 | 2.6099        | 0.11   | 2.6064      | 0           | 2.6064                  | -0.02 |         |       |
| 0.3    | 2.5252        | -3.14  | 2.5178      | 0.0892      | 2.6070                  | -0.00 | Fastcap |       |
| 0.5    | 1.9698        | -24.44 | 1.9692      | 0.6330      | 2.6022                  | -0.19 | 2.607   |       |
| 0.7    | 1.5779        | -39.48 | 1.5784      | 1.0271      | 2.6055                  | -0.06 |         |       |

instead of by (2.10), by the following formula:

$$\Sigma_{LP} = \frac{3}{2a} \frac{N_{\text{inf}} + N_I + N_{III} + N_{IV}}{N_{\text{path-LP}}}, \quad (4.18)$$

where  $N_{\text{inf}}$ ,  $N_I$ ,  $N_{III}$ , and  $N_{IV}$  represent the number of particles which finally go to infinite, plate I, III, and IV, respectively.  $N_{\text{path-LP}}$  denotes the total number of Brownian pathes starting from the hemisphere  $\Gamma$ .

From Table 4.3. we can see that when the radius  $a \leq 0.2773$ , the disk  $S_a$  is totally inside the plate II, and the last-passage method is correct with a maximal relative error less 0.17%. However, once  $S_a$  becomes larger and covers areas of plates with different potentials, the relative errors of the last passage method increases and even up to  $-39.48\%$ . In comparison, the BIE-WOS

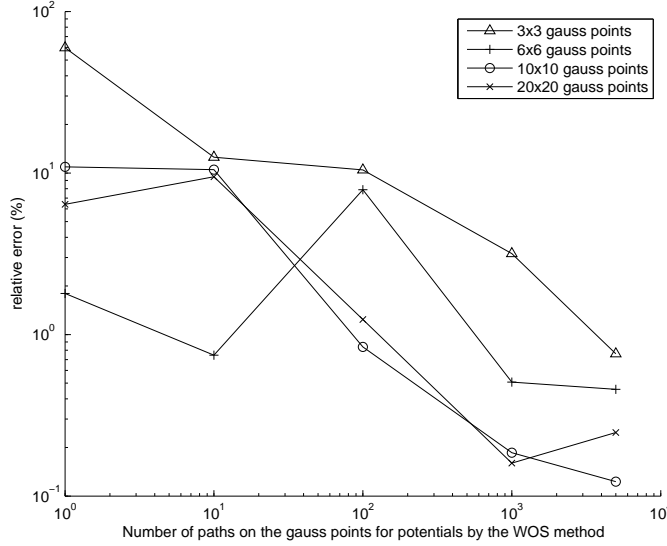


FIG. 4.3. *Convergence of BIE-WOS vs number of Brownian pathes and Gauss points*

maintains its accuracy insensitive to the radius  $a$  with a maximal relative errors less than  $-0.19\%$  as the radius varies from 0.1 to 0.7. This again confirms the fact that the last-passage method of [14] is designed for conducting surfaces (i.e., constant potential), not for surface of variable potentials. Therefore, it should not be used when the disk  $S_a$  includes regions of different potentials.

In conclusion, for a general variable potential, the last passage method is limited while the BIE-WOS does not suffer from the constrain of a constant boundary potential.

- *Test 3: Four rectangle plates with a complex potential distribution*

To further emphasize the point raised above in Test 2, we set the four plates with a complex potential distribution as:

$$\phi(x, y) = \sin mx \sin ny. \quad (4.19)$$

To obtain an accurate result, the last-passage method will require increasingly smaller radius  $a$  for ever larger  $m$  and  $n$  to achieve an (approximately) constant potential within the disk  $S_a$ .

The charge density at the point  $(-0.5, 0.5)$  by the last-passage, BIE-WOS and DBEM are shown in Table 4.4. We take the result of DBEM with  $17 \times 17$  panels on each plate as the reference solution. All other parameters in BIE-WOS and last passage methods are same as in the previous case. From Table 4.4, we can see that the BIE-WOS is more accurate.

The relative errors versus the number of Gauss points and the WOS paths are shown in Fig. 4.3. The BIE-WOS result of  $N_{g1} \times N_{g1} = 20 \times 20$ ,  $N_{g2} \times$

TABLE 4.4  
CHARGE DENSITY OF A FOUR UNIT PLATES STRUCTURE WITH COMPLEX  
VOLTAGES IN DIFFERENT RADIUS

| $a$ | Last passage  |      | BIE-WOS     |             |                         |      | DBEM    |
|-----|---------------|------|-------------|-------------|-------------------------|------|---------|
|     | $\Sigma_{LP}$ | err% | $\Sigma'_1$ | $\Sigma'_2$ | $\Sigma'_1 + \Sigma'_2$ | err% | value   |
| 0.1 | -0.4522       | 3.92 | -0.4454     | -0.008617   | -0.4540                 | 3.54 | -0.4707 |
| 0.2 | -0.4442       | 5.62 | -0.4444     | -0.01722    | -0.4616                 | 1.93 |         |
| 0.3 | -0.4369       | 7.17 | -0.4362     | -0.02579    | -0.4620                 | 1.85 |         |
| 0.4 | -0.4288       | 8.90 | -0.4278     | -0.03433    | -0.4621                 | 1.82 |         |
| 0.5 | -0.4203       | 10.7 | -0.4202     | -0.04280    | -0.4630                 | 1.62 |         |

$N_{g2} = 10 \times 10$  and  $N_{path} = 2 \times 10^3$  and  $a = 0.5$  is taken as the reference solution. From Fig. 4.3, we can see that when the number of the Brownian paths  $N_{path}$  is larger than  $10^2$  at each Gauss point, the BIE-WOS result with  $10 \times 10$  Gauss points will reach an accuracy about 1% in relative error.

• *Test 4: CPU time comparison with last-passage method*

For both the last-passage and BIE-WOS methods, the CPU time is expected to be linear in terms of the total number of random paths. We demonstrate this fact with a case of a thin circular disk with radius  $b$  case in 3-D space [14] as shown in Fig. 4.4. From [15], the analytic result of the charge density on the disk is:

$$\sigma(\rho) = \frac{Q}{4\pi b \sqrt{b^2 - \rho^2}}, \quad Q = 8b. \quad (4.20)$$

For a given relative error tolerance on the charge density at  $(-0.5, 0, 0)$ , the CPU time comparison of both methods versus the number of random paths are listed in Table 4.5. We take the radius  $a = 0.4$  for  $S_a$ ,  $b = 1$  for the radius of the thin disk, and the analytic charge density is  $\sigma(0.5) = 0.735105$ . From Table 4.5, we can see that the CPU times are indeed in proportion to total number of random paths for both methods for a comparable accuracy. Though the integral  $\Sigma'_2$  of the BIE-WOS method in this case is obviously zero, we still evaluate it just as for a general variable potential and the CPU time of  $\Sigma'_2$  is included in the CPU time of the BIE-WOS method in Table 4.5. It is noted that the CPU time in computing the integral  $\Sigma'_2$  for all cases are insignificant at about 0.012 second for a  $20 \times 20$  Gauss quadrature.

**4.2. Finding Neumann data over a patch of a curved boundary.**

Next, to test the BIE-WOS method for a curved boundary, we compute the DtN mapping on a big sphere as shown in Fig. 4.4 with a radius  $R = 3$ . A point charge  $q = 1$  is located at the central point  $O$  and the analytic result for the potential is then known. To compute the Neumann data over a local patch  $S$  around the point  $\mathbf{o} = (0, 0, 3)$  on the big spherical surface, a small

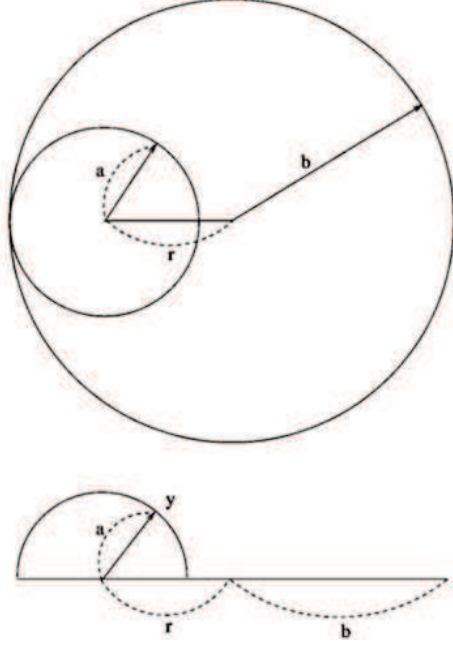


FIG. 4.4. Finding the charge distribution over a disk in 3-D

TABLE 4.5

THE RELATIVE ERRORS AND THE CPU TIMES COMPARISON ACCORDING TO THE NUMBER  $N$  OF RANDOM PATHS

| Last passage (LP)    |                      |       |             | BIE-WOS                          |                         |       |             |
|----------------------|----------------------|-------|-------------|----------------------------------|-------------------------|-------|-------------|
| $N_{\text{path-LP}}$ | $\Sigma_{\text{LP}}$ | err%  | cpu time(s) | $N_{\text{path-bie-wos}}$        | $\Sigma'_1 + \Sigma'_2$ | err%  | cpu time(s) |
| $10^4$               | 0.69975              | -4.81 | 32          | $10^2 \cdot 100 = 10^4$          | 0.68888                 | -6.29 | 30          |
| $10^5$               | 0.73253              | -0.35 | 331         | $10^2 \cdot 1000 = 10^5$         | 0.73960                 | 0.61  | 307         |
| $4 \cdot 10^5$       | 0.73743              | 0.32  | 1325        | $20^2 \cdot 1000 = 4 \cdot 10^5$ | 0.73441                 | -0.09 | 1218        |

sphere with a radius  $a = 1$  is superimposed over the point  $\mathbf{o}$ . The local patch  $S$  is discretized with a triangular mesh as shown in Fig. 4.5.

The BIE equation of (3.2) is solved by a collocation boundary element method. When the collocation point is not inside an integration panel of the BEM, a simple Gauss quadrature method is used. For collocation point inside an integration panel, both weak and strong singularities will occur, however, they can be regularized by a local polar transformation technique and a  $20 \times 20$  Gauss quadrature will then be used. For the integrals on  $\Gamma$ , a  $30 \times 30$  Gauss quadrature will be used. The potential  $u(\mathbf{y})$  on  $\Gamma$  is first computed, by the Feynman-Kac formula and the WOS method with  $10^4$  Brownian paths, on a regular grid, which is generated by evenly discretizing the spherical surface along the polar and azimuthal angles. The value  $u(\mathbf{y})$  at other locations on  $\Gamma$

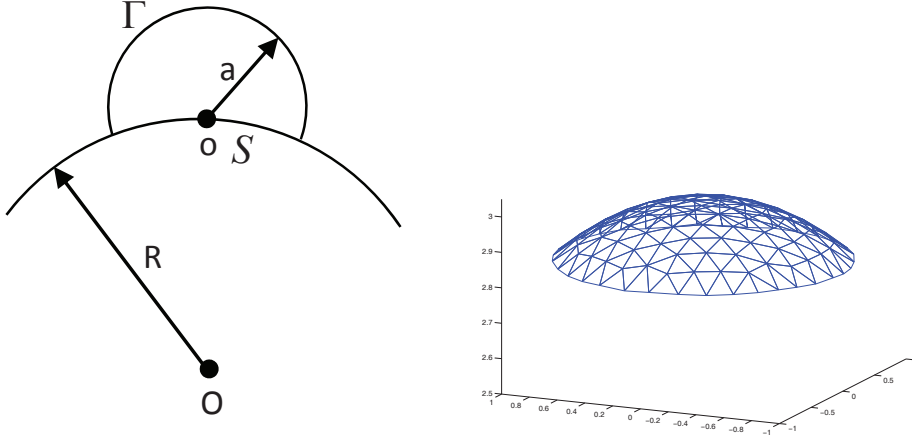


FIG. 4.5. Left: BIE-WOS setting for finding Neumann data over a patch of a bigger sphere; right: the mesh over the patch

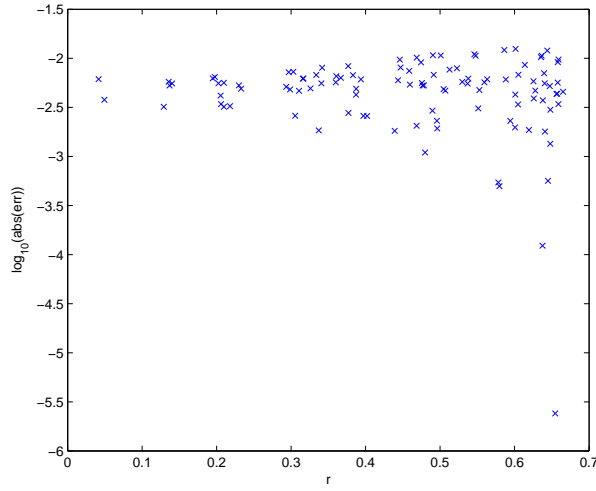


FIG. 4.6. Accuracy of the Neumann data by the BIE-WOS over the patch  $S$ ,  $r < 0.7a$ ,  $a$  is the radius of  $\Gamma$ .

as required by numerical quadratures will be interpolated using the values on the grid points.

The relative errors at the center of triangular panels on  $S$  are shown in Fig. 4.6, where  $x$ -axis means the distance between the triangle center to point  $\mathbf{o}$ . From Fig. 4.6, we can see that for the panels close to point  $\mathbf{o}$ , i.e.  $r < 0.7a$ , the maximal relative error is less than 1.25%, which will be accurate enough for most engineering applications. It is noted that due to the sharp corner

edge singularity of the domain  $\Omega_S$  where the hemisphere and  $\partial\Omega$  intersect, the collocation BEM will lose some of its accuracy, which limits the region where acceptable accuracy of the BEM solution can be used for the sought-after Neumann data. This well known problem in singular boundary elements usually is addressed with graded mesh near the edge singularity [6][1][19] and still an active research topic in BEM methods [4]. A resolution of this edge singularity can increase of the region of useful BEM solution in the BIE-WOS algorithm and can be incorporated into the algorithm. As discussed in the last section, as the boundary  $\partial\Omega$  will be covered with an overlapping patches  $S_i$ , the loss of the accuracy of the BIE solution near the edge of each patch will not hinder the use of the BIE-WOS method. However, any improvement of the BEM near the edge will reduce the total number of patches to cover the boundary, thus reducing the total cost.

**5. Conclusion and discussions.** In this paper we have proposed a local BIE-WOS method which combines a local deterministic singular boundary integral equation method and the Monte Carlo WOS algorithm to find the Neumann data on general surfaces given Dirichlet data there. The singular integral equation for the Neumann data at any single point or a local patch on the boundary surface involves potential solution on a local hemisphere, which can be readily obtained with Feynman-Kac formula with the help of WOS sampling of the Brownian pathes. Numerical results validate the efficiency and accuracy of this method.

The local BIE-WOS method of finding the DtN or NtD mapping can give a parallel algorithm for the solution of the Poisson equation with Dirichlet or Neumann boundary conditions. Firstly, we partition the whole boundary  $\partial\Omega$  into a union of overlapping pathes  $S_i$  namely,

$$\partial\Omega = \cup_i S_i,$$

then, the local BIE-WOS can be used to find the DtN or NtD mapping over each patch  $S_i$  independently in parallel. In principle, the computation of BIE-WOS over each patch can be done over one computing processor without need for communications with others, thus a high parallel scalability can be achieved. Secondly, the solution to the Poisson equation in the whole space can be found with the integral representation of (1.3) with the help of one application of FMM [13].

There are several important research issues to be addressed before the BIE-WOS method can be used for large scale computation of Poisson or modified Helmholtz equations, including (1) the NtD mapping problem, where the Neumann data is given on the boundary and the Dirichlet data is required. In this case, the Feynman-Kac formula derived in [18] can be used, which will involve reflecting Brownian pathes [20] with respect to the domain boundary. Efficient numerical implantation will have to be developed; (2) Modified

Helmholtz equation, even though the Feynman-Kac formula (1.7) still applies, a survival factor will be introduced as the WOS samples the Brownian paths and efficient way to use the Feynman-Kac formula will be addressed; and (3) the WOS scheme requires the computation of the distance between a Brownian particle and the boundary of the solution domain, efficient algorithms will be studied for the overall speed of the BIE-WOS method.

The BIE-WOS based-parallel algorithm for solving Poisson or modified Helmholtz equation will have the following important features:

- Non-iterative in construction and no need to solve any global linear system.
- Stochastic in nature based on the fundamental link between Brownian motion and the solution of elliptic PDEs.
- Massive parallelism suitable to large number of processors for large scale computing due to the random walk and local integral equation components of the algorithm.
- No need for traditional finite element type surface or volume meshes.
- Applicable to complex 3-D geometry with high accuracy treatment of domain boundary geometries.

In comparison with traditional finite element and finite difference methods, the BIE-WOS based solver is only suitable for Poisson and modified Helmholtz equations (due to the use of WOS-type sampling technique of the diffusion paths) and its accuracy is limited to that of the Monte Carlo sampling technique, while the traditional grid based method can handle more general variable coefficients PDEs and achieve high accuracy. Nonetheless, as the Poisson and modified Helmholtz equations form the bulk computation of projection-type methods for incompressible flows and other important scientific computing, the progress in scalability of parallel BIE-WOS based-solvers will have large impact on the simulation capability of incompressible flow and engineering applications.

### **Acknowledgement**

The first and third authors are supported in part by NSFC research projects 60976034 and 61076033, the National Basic Research Program of China under the grant 2011CB309701, the National major Science and Technology special project 2009ZX02023-4-3 of China during the 11-th five-year plan period, the National major Science and Technology special project 2011ZX01034-005-001-03 of China during the 12-th five-year plan period, the Doctoral Program Foundation of the Ministry of Education of China 200802460068, the Program for Outstanding Academic Leader of Shanghai. The State Key Lab. of ASIC & System Fudan Univ. research project 11MS013.

## REFERENCES

- [1] K. Atkinson & Graham, I. Iterative variants of the Nyström method for second kind boundary integral operators, *SIAM J. Sci. Stat. Comput.* 13, (1990), 694–722.
- [2] C. A. Brebbia, The boundary element method in engineering. Pentech Press. London, 1978.
- [3] A. Brandt, Guide to multigrid development, *Lecture Notes in Mathematics*, 1982, Volume 960/1982, 220–312.
- [4] J. Bremer, V. Rokhlin, Efficient discretization of Laplace boundary integral equations on polygonal domains, *Journal of Computational Physics*, V. 229, (2010), Pages 2507–2525.
- [5] A.J. Chorin, Numerical solution of the Navier–Stokes equations, *Math. Comput.* 22 (1968) 745–762.
- [6] G. Chandler Galerkin’s method for boundary integral equations on polygonal domains, *J. Austral. Math. Soc., Ser. B* 26, (1984) 1–13.
- [7] G. Chen and Zhu, H. and Cui, T. and Chen, Z. and Zeng, X. and Cai, W. ParAFEM-Cap: A Parallel Adaptive Finite-Element Method for 3-D VLSI Interconnect Capacitance Extraction. *IEEE Trans. on Microwave Theory and Techniques*, no. 9, pp. 218–231, 2012.
- [8] Y. Coz and R. B. Iverson, “A stochastic algorithm for high speed capacitance extraction in integrated circuits,” *Solid-State Electron.*, vol. 35, no. 7, pp. 1005–1012, July 1992.
- [9] Y. Coz, H. J. Greub, and R. B. Iverson, “Performance of randomwalk capacitance extractors for IC interconnects: A numerical study,” *Solid-State Electron.*, vol. 42, no. 4, pp. 581–588, April 1998.
- [10] K. L. Chung, Green, Brown and Probability, world scientific, 1995.
- [11] M. Freidlin, Functional Integration and Partial Differential Equations, Princeton University Press, 1985.
- [12] A. Friedman, Stochastic differential equations and applications, Dover publication, 2006.
- [13] L. Greengard, V. Rokhlin, A fast algorithm for particle simulations, *J. Comput. Phys.* 73 (1987) 325.
- [14] J. A. Given, Chi-Ok Hwang and Michael Mascagni, First- and last-passage Monte Carlo algorithms for the charge density distribution on a conducting surface. *PHYSICAL REVIEW E* 66, 056704 ~2002
- [15] J. A. Given, Chi-Ok Hwang. Edge distribution method for solving elliptic boundary value problems with boundary singularities. *PHYSICAL REVIEW E* 68, 046128 2003
- [16] J. Giroire & J. C. Nédélec, J. C. Numerical solution of an exterior neumann problem using a double layer potential, *Math. Comp.* 32, (1978), 973–990.
- [17] C. O. Hwang and James A. Given, Last-passage Monte Carlo algorithm for mutual capacitance, *PHYSICAL REVIEW E* 74, 027701 2006.
- [18] P. Hsu, Probabilistic approach to the Neumann problem, *Comm. Pure and App. Math.*, vol38, 445–472 (1985).
- [19] R. A. Kress, A Nyström method for boundary integral equations in domains with corners, *Numer. Math.* 58, (1990), 145–161.
- [20] P.L. Lions and A. S. Sznitman, Stochastic differential equations with reflecting boundary conditions, *Communications on Pure and Applied Mathematics*, Vol. XXXVII, 511–537 (1984).
- [21] M. Mascagni and C. O. Hwang,  $\epsilon$ -shell error analysis for “Walk on spheres” algorithms, *Mathematics and Computer in Simulations* 63 (2003) 93–104.
- [22] M.E. Muller, Some continuous Monte Carlo methods for the Dirichlet problem. *The Annals of Mathematical Statistics*. vol. 27(3), pp.569–589, 1956.
- [23] M. Mascagni and Simonov, N.A. The random walk on the boundary method for calcu-



- lating capacitance. *Journal of Computational Physics*, vol.195(2004), pp. 465-473.
- [24] K. Nabors and J. White, "FastCap: A multipole accelerated 3-D capacitance extraction program,"
  - [25] J. Phillips and J. White, "A Precorrected-FFT Method For Capacitance Extraction of Complicated 3-D Structures," in *Proc. IEEE/ACM Int.Conf. Computer-Aided Design*, Nov. 1994, pp. 268 -271.
  - [26] W. Shi, J. Liu, N. Kakani, and T. Yu, "A fast hierarchical algorithm for three-dimensional capacitance extraction," *IEEE Trans. Comput.- Aided Des. Integr. Circuits Syst.*, vol. 21, no. 3, pp. 330-336, Mar. 2002.
  - [27] R. Temam, *Navier-Stokes Equations: Theory and Numerical Analysis*, North-Holland, Amsterdam, 1984
  - [28] S. Yan, V. Sarim, and W. Shi, "Sparse transformation and preconditioners for 3-D capacitance extraction," *IEEE Trans. Comput.-Aided Des. Integr. Circuits Syst.*, vol. 24, no. 9, pp. 1420-1426, Sep. 2005.
  - [29] W. Yu, and Zeyi Wang, Enhanced QMM-BEM Solver for Three-Dimensional Multiple-Dielectric Capacitance Extraction Within the Finite Domain. *IEEE TRANSACTIONS ON MICROWAVE THEORY AND TECHNIQUES*, VOL. 52, NO. 2, FEBRUARY 2004 pp.560-566.
  - [30] O. Widlund, *Domain decomposition methods-algorithms as well as theory*, Springer, 2005.